This is a preprint, the final version is subject to change, of the American Mineralogist (MSA)
Cite as Authors (Year) Title. American Mineralogist, in press.
(DOI will not work until issue is live.) DOI: http://dx.doi.org/10.2138/am.2014.4844

Ichnusaite, $Th(MoO_4)_2 \cdot 3H_2O$, the first natural thorium molybdate: occurrence, description, and crystal structure

PAOLO ORLANDI[1,2], CRISTIAN BIAGIONI[1,*], LUCA BINDI[3], AND FABRIZIO NESTOLA[4]

[1] *Dipartimento di Scienze della Terra, Università di Pisa, Via S. Maria 53, I-56126 Pisa, Italy*
[2] *Istituto di Geoscienze e Georisorse, CNR, Via Moruzzi 1, I-56124 Pisa, Italy*
[3] *Dipartimento di Scienze della Terra, Università degli Studi di Firenze, Via G. La Pira, 4, I-50121 Firenze, Italy*
[4] *Dipartimento di Geoscienze, Università di Padova, Via Gradenigo, 6, I-35131 Padova, Italy*

**e-mail address*: biagioni@dst.unipi.it

This is a preprint, the final version is subject to change, of the American Mineralogist (MSA)
Cite as Authors (Year) Title. American Mineralogist, in press.
(DOI will not work until issue is live.) DOI: http://dx.doi.org/10.2138/am.2014.4844

ABSTRACT

The new mineral species ichnusaite, $Th(MoO_4)_2 \cdot 3H_2O$, has been discovered in the Mo-Bi mineralization of Su Seinargiu, Sarroch, Cagliari, Sardinia, Italy. It occurs as colorless thin {100} tabular crystals, up to 200 μm in length, associated with muscovite, xenotime-(Y), and nuragheite, $Th(MoO_4)_2 \cdot H_2O$. Luster is pearly-adamantine. Ichnusaite is brittle, with a perfect {100} cleavage. Owing to the very small quantity of available material and its intimate association with nuragheite, density and optical properties could not be measured. Electron microprobe analysis gave (wt% - mean of 4 spot analyses): MoO_3 47.86(1.43), ThO_2 43.40(79), total 91.26(87). On the basis of 8 O atoms per formula unit and assuming 3 H_2O groups, in agreement with the crystal structure data, the chemical formula of ichnusaite is $Th_{0.99}Mo_{2.01}O_8 \cdot 3H_2O$. Main diffraction lines, corresponding to multiple *hkl* indices, are [*d*(Å), relative visual intensity]: 5.66 (m), 3.930 (m), 3.479 (s), 3.257 (s), 3.074 (m). Ichnusaite is monoclinic, space group $P2_1/c$, with *a* 9.6797(12), *b* 10.3771(13), *c* 9.3782(12) Å, β 90.00(1)°, *V* 942.0(2) Å^3, *Z* = 4. The crystal structure has been solved and refined to a final R_1 = 0.051 on the basis of 2008 observed reflections [with $F_o > 4\sigma(F_o)$]. It consists of electroneutral $[Th(MoO_4)_2(H_2O)_2]^0$ (100) sheets of polymerized $ThO_7(H_2O)_2$ and MoO_4 polyhedra; successive sheets, stacked along [100], are connected through hydrogen bonds. Ichnusaite brings new understanding about the crystal chemistry of actinide molybdates, that may form during the alteration of spent nuclear fuel and influence the release of radionuclides under repository conditions.

Keywords: ichnusaite, new mineral species, molybdate, thorium, crystal structure, Su Seinargiu, Sardinia, Italy.

Introduction

Thorium (Z = 90) is an actinide element found in the bulk silicate Earth with the estimated average concentration of ~ 0.06 ppm (Plant et al. 1999); even if it is about three times more abundant than uranium, only twenty-two mineral species containing Th as an essential component are known (Table 1), compared to more than 200 uranium mineral species. This difference is discussed by Hazen et al. (2009) and related to three main aspects: i) Th occurs only as Th^{4+} and it does not have an analog of $(UO_2)^{2+}$ ion, not forming isomorphs of the numerous uranyl compounds; ii) the half-life of ^{232}Th (the most abundant isotope of Th) is ~ 14 billion years so that thorium minerals do not show extensive degree of radiation damage and chemical alteration; and iii) Th-compounds are relatively insoluble, and Th^{4+} is mobilized under much more restricted chemical-physical conditions than U^{4+}, not being complexed by chloride or carbonate (as occurs for U^{4+}) but only forming F-complexes. Thorium occurs as a minor component in rare-earth element phosphates (e.g., monazite, xenotime) and as a trace element in apatite–group minerals (Luo et al. 2011); owing to its occurrence in these common rock-accessory phases, Th minerals can be used as geochronometers for dating through the U-Th-Pb and (U,Th)/He methods.

During a routine check of mineral samples from Su Seinargiu (Sardinia, Italy) through qualitative EDS chemical analyses, some crystals were identified containing only Th and Mo. Up to now, natural thorium molybdates were unknown and consequently X-ray diffraction studies were performed in order to completely characterize this new compound. X-ray powder diffraction patterns collected through a Gandolfi camera revealed the presence of two different Th-Mo phases. Single-crystal X-ray diffraction studies showed that these two phases commonly form intimate intergrowths, making difficult their mineralogical study. Through the examination of several crystals, two pure grains of both phases were identified, allowing the intensity data collection and solution of the two crystal structures. The two Th-Mo phases, differing in their hydration states, were proposed as new minerals.

In this paper we describe the first of these two natural thorium molybdates, which was named ichnusaite (pronounced *iknusa-ait*). The name is from the old Greek name of Sardinia, *Ιχνουσσα, ichnusa*. The mineral and its name have been approved by the CNMNC-IMA under the number 2013-087. The holotype specimen of ichnusaite is deposited in the mineralogical collection of the Museo di Storia Naturale, Università di Pisa, Via Roma 79, Calci, Pisa, Italy, under catalog number 19679. The other new thorium molybdate, nuragheite, will be described in a separate paper (Orlandi et al. in preparation).

Geological setting

The occurrence of Mo minerals in Sardinia has been known since the second half of the 19th Century (Jervis 1881; Lovisato 1886; Traverso 1898). Numerous Mo mineralizations occur in close association with leucogranites of Variscan age (Ghezzo et al. 1981); Su Seinargiu is one of the smallest prospects. Its molybdenite mineralization has been dated by Boni et al. (2003) at 288.7 ± 0.5 My on the basis of Re-Os dating.

The Su Seinargiu prospect is located on the southern coast of Sardinia, northwest of the small town of Sarroch. Mineralization occurs within three vein systems hosted in leucogranite porphyry and embedded in slightly metamorphosed (greenschist facies) shales of Ordovician-Silurian age; veins are mainly composed of quartz and molybdenite. This latter mineral is also disseminated in the porphyry. A pervasive hydrothermal alteration is common throughout the intrusion, resulting in the widespread occurrence of clay minerals replacing plagioclase and K-feldspar.

In addition to molybdenite, Caboi et al. (1978) reported the occurrence of minor chalcopyrite, pyrite, and traces of "wolframite". Molybdenite is frequently altered in yellow ochres of molybdenum, indicated by Caboi et al. (1978) as molybdite. It is interesting to note that these authors stated that a peculiar feature of this mineralization is related to the small number of mineral species, with the mineral assemblage formed exclusively by quartz and molybdenite. On the contrary, Orlandi et al. (2013) described more than 50 mineral species from Su Seinargiu. Most of them are the results of the alteration of the primary Mo-Bi ore, composed of molybdenite, bismuthinite, and bismuth. In addition to ichnusaite, three other new mineral species have their type locality at Su Seinargiu: sardignaite (Orlandi et al. 2010), gelosaite (Orlandi et al. 2011), and tancaite-(Ce) (Bonaccorsi and Orlandi 2010).

Occurrence and mineral description

Ichnusaite occurs as aggregates of colorless thin {100} tabular crystals, up to 200 μm in length, with a pearly-adamantine luster. Streak is white. Ichnusaite is transparent, brittle, and shows a perfect cleavage parallel to (100).

Owing to the intimate intergrowths with nuragheite, $Th(MoO_4)_2 \cdot H_2O$, and the small amount of homogeneous material available, micro-indentation hardness, density, as well as the optical properties were not measured. The calculated density, based on the empirical formula, is 4.262 $g \cdot cm^{-3}$. The mean refractive index of ichnusaite, obtained from the

Gladstone-Dale relationship (Mandarino 1979, 1981) using the ideal formula and calculated density, is 1.92.

Ichnusaite is intimately intergrown with nuragheite, occurring within vugs of quartz veins, in association with muscovite and partially corroded crystals of xenotime-(Y). Its crystallization is probably related to the alteration of the molybdenite ore.

Chemical composition

One very small crystal of ichnusaite (20 μm for its largest dimension), not intergrown with nuragheite, was available and it was used for electron-microprobe analysis. Preliminary EDS chemical analysis showed Th and Mo as the only elements with $Z > 9$. Owing to the very small crystal size, only 4 spot analyses were carried out, using a CAMECA SX50 electron microprobe operating in WDS (wave-lenght dispersive) mode; operating conditions were as follows: accelerating voltage 20 kV, beam current 5 nA, beam size 1 μm. Standards used were (element, emission line): metallic Mo (Mo *L*α) and synthetic ThO_2 (Th *M*α). Electron microprobe data are given in Table 2. On the basis of 8 oxygen atoms per formula unit (*apfu*) and assuming the presence of three H_2O groups (as shown by the structural study), the chemical formula of ichnusaite can be written as $Th_{0.991}Mo_{2.006}O_8 \cdot 3H_2O$. The ideal formula is $Th(MoO_4)_2 \cdot 3H_2O$, corresponding to (in wt%) ThO_2 43.57, MoO_3 47.51, H_2O 8.92, sum 100.00.

X-ray crystallography and structure refinement

Single-crystal X-ray diffraction data were collected using a Bruker Smart Breeze diffractometer equipped with an air-cooled CCD area detector. Graphite-monochromatized Mo *K*α radiation was used. The detector-to-crystal distance was 50 mm. 774 frames were collected using φ and ω scan modes in 0.5° slices, with an exposure time of 5 seconds per frame. Data were integrated and corrected for Lorentz and polarization effects, background effects, and absorption, using the software package Apex2 (Bruke Axs Inc. 2004). The analysis of systematic absences unequivocally indicated the space group $P2_1/c$. Refined cell parameters are *a* 9.6797(12), *b* 10.3771(13), *c* 9.3782(12), β 90.00(1)°, *V* 942.0(2) $Å^3$, $Z = 4$. The crystal structure was solved through direct methods and refined using Shelx-97 (Sheldrick 2008). Scattering curves for neutral atoms were taken from the *International Tables for X-ray Crystallography* (Wilson 1992). Crystal data and details of the intensity data collection and refinement are reported in Table 3.

After locating the heavier atoms Th and Mo, some O positions were identified on the basis of difference-Fourier maps. However, at this stage, the analysis of the difference-Fourier map revealed large maxima around Th and Mo atoms and the R_1 was too high (0.27). Assuming a twinning on {100}, the R_1 dramatically decreased to 0.13, thus indicating the possible correctness of the structural model. The twin ratio of the two individuals is 0.49(1). Ichnusaite represents an archetypal example of twinning by metric merohedry according to Nespolo and Ferraris (2000).

Successive difference-Fourier maps allowed the correct location of all the oxygen atoms. After several cycles of isotropic refinements, an anisotropic model for all the atoms (with the exception of O7) was refined, achieving a final R_1 = 0.051 for 2008 observed reflections with $F_o > 4\sigma(F_o)$ and 0.060 for all 2223 independent reflections. The highest and deepest residuals are located around the Th atom and may be due to the low diffraction quality of the available crystal, i.e. broad diffraction peaks. Atomic coordinates and displacement parameters are given in Table 4 and Table 5 reports selected bond distances.

The X-ray powder diffraction pattern of ichnusaite was obtained using a 114.6 mm diameter Gandolfi camera, with Ni-filtered Cu *K*α radiation. The observed X-ray powder pattern is compared with the calculated one (obtained using the software Powder Cell; Kraus and Nolze 1996) in Table 6. Unit-cell parameters, refined on the basis of 20 unequivocally indexed reflections using UnitCell (Holland and Redfern 1997), are *a* 9.646(2), *b* 10.471(2), *c* 9.338(2) Å, β 90.34(2)°, *V* 943.2(2) Å^3.

Crystal structure description

The crystal structure of ichnusaite (Fig. 2) shows three independent cation sites, namely Th, Mo1, and Mo2, and eleven independent ligand sites. The cation-centered polyhedra are arranged in (100) layers, forming electroneutral $[Th(MoO_4)_2(H_2O)_2]^0$ sheets of polymerized $ThO_7(H_2O)_2$ and MoO_4 polyhedra. The sheets are linked by H bonding to interlayer H_2O (Ow11 site) groups and stacked along [100]; the H bonding involves O2, Ow6, Ow10, and Ow11 sites, as suggested by the examination of O···O distances shorter than 3.0 Å which are not polyhedral edges (Table 7) and bond-valence calculation (Table 8).

Thorium atoms are bonded to seven oxygen atoms and two H_2O groups in a tricapped trigonal prismatic coordination. Average <Th–O> bond distance is 2.459 Å, in agreement with ideal Th–O distance of 2.44 Å, assuming the ionic radii given by Shannon (1976). Every Th-centered polyhedron shares corners with seven Mo-centered tetrahedra. The Mo1 tetrahedron shares corners with four Th-centered polyhedra, whereas the Mo2 tetrahedron

shares corners with three Th polyhedra. The free vertex of the Mo2 tetrahedron (O2 site) is at hydrogen bond distance with H_2O groups belonging to two distinct Th polyhedra, namely Ow6 and Ow10 sites. Average <Mo–O> bond distances are 1.751 and 1.768 Å for Mo1 and Mo2 sites, respectively.

As reported above, O···O distances shorter than 3.0 Å suggest the presence of hydrogen bonds. Figure 3 shows the proposed hydrogen bond network connecting successive $[Th(MoO_4)_2(H_2O)_2]^0$ sheets as seen down **c**. The connection is achieved through the bonds Ow10···O2 and Ow6···Ow11···Ow10; the former involves the interlayer H_2O groups and forms an angle of 111.8(9)°. In addition to hydrogen bonds connecting successive layers, the short O···O distance between Ow6 and O2, which occupies the free vertex of Mo2 tetrahedron in the same sheet, suggests an intrasheet hydrogen bond between the Mo2 and Th polyhedra.

Discussion

The term molybdate indicates a compound containing an oxoanion with molybdenum in its highest oxidation state +6. Molybdenum can form a large range of oxoanions, e.g., $(MoO_4)^{2-}$ and $(Mo_2O_7)^{2-}$. Forty-eight minerals contain Mo as an essential component; among them, twelve valid species are characterized by the oxoanion $(MoO_4)^{2-}$ (Table 9). One potential new mineral species, never submitted to the formal IMA approval, is represented by the phosphate analogue of molybdofornacite described by Nickel and Hitchen (1994). Among the phases reported in Table 9, it should be noted that the crystal structure of ferrimolybdite has not been solved yet, so the presence of the $(MoO_4)^{2-}$ oxoanion is speculative. Deloryite, $Cu_4(UO_2)(MoO_4)_2(OH)_6$, and umohoite, $(UO_2)MoO_4{\cdot}2H_2O$, have chemical formulas showing (MoO_4) groups; however, Mo has five-fold and six-fold coordinations, respectively, in those structures (Pushcharovsky et al. 1998; Krivovichev and Burns 2000). Taking into account the usual five-fold and six-fold Mo coordination in all U molybdates known so far, sedovite, ideally $U(MoO_4)_2$ (Skvortsova and Sidorenko 1965), is not reported in Table 9, owing to the lack of structural data and the consequent uncertainties about the actual Mo coordination in such mineral.

Ichnusaite fits the 07.GB group of Strunz and Nickel classification; i.e., molybdates with additional anions and/or H_2O (Strunz and Nickel 2001). Whereas eight mineral species contain Mo and U, no Th molybdates were known: ichnusaite is the first natural thorium molybdate to be described. Among synthetic compounds, two polymorphic phases of anhydrous $Th(MoO_4)_2$ are known, having orthorhombic and trigonal symmetry, respectively (Cremers et al. 1983; Larson et al. 1989). Ichnusaite shows a new type of layered structure;

the relations between this structure and those of nuragheite and synthetic $Th(MoO_4)_2$ will be described elsewhere (Orlandi et al., in preparation).

Ichnusaite is likely the product of the alteration of the primary Mo-Bi ore at Su Seinargiu under basic pH conditions. In fact, according to Birch et al. (1998), phases with tetrahedral $(MoO_4)^{2-}$ oxoanions could form at pH 7-8, under more basic conditions than do species with octahedrally coordinated Mo. Molybdenite could be the source of Mo at Su Seinargiu, whereas the occurrence of corroded crystals of xenotime-(Y) suggests that this REE phosphate, isostructural with thorite, $ThSiO_4$, might the source of Th. Indeed, some authors reported high Th concentrations in xenotime-(Y) (e.g., Förster 2006).

Implications

Thorium, as well as uranium, has a special importance to geoscientists. In fact, the energy released by their radioactive decay has driven the thermal evolution of Earth, resulting in the layering of Earth's internal structure and plate tectonics. As is well known, the radioactive decay of ^{232}Th, as well as ^{238}U and ^{235}U, to stable Pb isotopes provided the basis for geochronological measurements providing absolute ages for the geologic time scale. Moreover, in agreement with Hazen et al. (2009), the mineralogy of uranium and thorium can provide a measure of planets' geotectonic and geobiological history.

In addition to its geological importance, thorium has extensive industrial applications, e.g., as an alloying agent in gas tungsten arc welding to increase the melting temperature of tungsten electrodes (Cary and Helzer 2005) or as a catalyst in the conversion of NH_3 to HNO_3 and the production of H_2SO_4 (Patnaik 2003). Moreover, thorium has been tentatively used in the production of energy in nuclear plants and for the production process of the fissile isotope ^{233}U. Owing to its natural abundance, attractive physical, chemical, and nuclear properties, there is an increasing interest in the thorium fuel cycle (e.g., Lung and Gremm 1998; Ünak 2000). Consequently, the disposal of thorium waste is an important environmental issue (e.g., Luo et al. 2011).

Owing to the fact that molybdenum is one of the many fission products in a nuclear reactor, the formation of actinide molybdates has been reported during the alteration of spent nuclear fuel (e.g., Buck et al. 1997), under conditions similar to those expected in the once-proposed geological repository at Yucca Mountain, Nevada, U.S.A. Ichnusaite, being a new structure type among actinide molybdates, brings new data to the understanding of the crystal chemistry of such compounds, potentially useful for understanding the release of radionuclides under repository conditions.

Acknowledgements

The first specimen of ichnusaite was provided by Giuseppe Tanca; other specimens were given by Fernando Caboni, Marzio Mamberti, and Antonello Vinci. We are grateful to all these Sardinian mineral collectors for their efforts in the sampling of the Su Seinargiu prospect. Electron microprobe analyses were performed with the help of Raul Carampin; we are grateful to Leonardo Tauro and Elena Masiero for the preparation of the sample for electron microprobe analysis. The paper was handled by Peter Burns and benefited of the comments of the two reviewers Robert Finch and Sergey Krivovichev.

References

Aleksandrov, V.B., Gorbatyii, L.V., and Ilyukhin, V.V. (1968) Crystal structure of powellite $CaMoO_4$. Soviet Physics – Crystallography, 13, 414–415.

Berlepsch, P., Armbruster, T., Brugger, J., Bykova, E.Y., and Kartashov, P.M. (1999) The crystal structure of vergasovaite $Cu_3O[(Mo,S)O_4SO_4]$, and its relation to synthetic $Cu_3O[MoO_4]_2$. European Journal of Mineralogy, 11, 101–110.

Birch, W.D., Pring, A., McBriar, E.M., Gatehouse, B.M., and McCammon, C.A. (1998) Bamfordite, $Fe^{3+}Mo_2O_6(OH)_3 \cdot H_2O$, a new hydrated iron molybdenum oxyhydroxide from Queensland, Australia: Description and crystal chemistry. American Mineralogist, 83, 172–177.

Bonaccorsi, E. and Orlandi, P. (2010) Tancaite-(Ce), a new molybdate from Italy. Acta Mineralogica Petrographica Abstract Series. 20th General Meeting of the International Mineralogical Association, 21st-27th August, 2010. Budapest, Hungary, 6, 494.

Boni, M., Stein, H.J., Zimmerman, A., and Villa, I.M. (2003) Re-Os age for molybdenite from SW Sardinia (Italy): A comparison with $^{40}Ar/^{39}Ar$ dating of Variscan granitoids. Mineral Exploration and Sustainable Development, Eliopoulos et al. (ed), 247–250.

Brese, N.E. & O'Keeffe, M. (1991): Bond-valence parameters for solids. Acta Crystallographica, B47, 192–197.

Bruker AXS Inc. (2004) APEX 2. Bruker Advanced X-ray Solutions, Madison, Wisconsin, USA.

Buck, E.C., Wronkiewicz, D.J., Finn, P.A., and Bates, J.K. (1997) A new uranyl oxide hydrate phase derived from spent fuel alteration. Journal of Nuclear Materials, 249, 70–76.

Burns, P.C. (1998) The crystal structure of szenicsite, $Cu_3MoO_4(OH)_4$. Mineralogical Magazine, 62, 461–469.

Caboi, R., Massoli-Novelli, R., and Sanna, G. (1978) La mineralizzazione a molibdenite di P.ta de Su Seinargiu (Sarroch – Sardegna meridionale). Rendiconti della Società Italiana di Mineralogia e Petrologia, 34, 167–186.

Calvert, L.D. and Barnes, W.H. (1957) The structure of lindgrenite. The Canadian Mineralogist, 6, 31–51.

Cary, H. and Helzer, S. (2005) Modern Welding Technology, Prentice Hall, New Jersey.

Cremers, T.L., Eller, P.G., and Penneman, R.A. (1983) Orthorhombic Thorium(IV) Molybdate, $Th(MoO_4)_2$. Acta Crystallographica, C39, 1165–1167.

Ferraris, G. and Ivaldi, G. (1988) Bond valence vs bond length in O···O hydrogen bonds. Acta Crystallographica, B44, 341–344.

Förster, H.-J. (2006) Composition and origin of intermediate solid solutions in the system thorite-xenotime-zircon-coffinite. Lithos, 88, 35–55.

Ghezzo, C., Guasparri, G., Riccobono, F., Sabatini, G., Pretti, S., and Uras, I. (1981) Le mineralizzazioni a molibdeno associate al magmatismo intrusivo ercinico della Sardegna. Rendiconti della Società Italiana di Mineralogia e Petrologia, 38, 133–145.

Hazen, R.M., Ewing, R.C., and Sverjensky, D.A. (2009) Evolution of uranium and thorium minerals. American Mineralogist, 94, 1293-1311.

Holland, T.J.B. and Redfern, S.A.T. (1997) Unit cell refinement from powder diffraction data: the use of regression diagnostics. Mineralogical Magazine, 61, 65–77.

Horn, E., Kurahashi, M., Huang, D., and Wu, C. (1995) Crystal data and X-ray powder-diffraction data for ferrimolybdite, $Fe_2(MoO_4)_3 6.8H_2O$. Powder Diffraction, 10, 101–103.

Jervis, G. (1881) I tesori sotterranei d'Italia. Parte Terza: Regione delle isole Sardegna e Sicilia e addenda ai precedenti volumi. Ermanno Loescher Ed., Torino, 539 pp.

Kraus, W. and Nolze, G. (1996) Powder Cell – a program for the representation and manipulation of crystal structures and calculation of the resulting X-ray powder patterns. Journal of Applied Crystallography, 29, 301–303.

Krivovichev, S. and Burns, P.C. (2000) Crystal chemistry of uranyl molybdates. I. The structure and formula of umohoite. The Canadian Mineralogist, 38, 717–726.

Larson, E.M., Eller, P.G., Cremers, T.L., Penneman, R.A., and Herrick, C.C. (1989) Structure of trigonal thorium molybdate. Acta Crystallographica, C45, 1669–1672.

Lovisato, D. (1886) Contributo alla mineralogia sarda. Rendiconti dell'Accademia Nazionale dei Lincei, 2, 254-259.

Lung, M. and Gremm, O. (1998) Perspectives of the thorium fuel cycle. Nuclear Engineering and Design, 180, 133–146.

Luo, Y., Rakovan, J., Tang, Y., Lupulescu, M., Hughes, J.M., and Pan, Y. (2011) Crystal chemistry of Th in fluorapatite. American Mineralogist, 96, 23–33.

Mandarino, J.A. (1979) The Gladstone-Dale relationship. Part III. Some general applications. The Canadian Mineralogist, 17, 71–76.

Mandarino, J.A. (1981) The Gladstone-Dale relationship. Part IV. The compatibility concept and its application. The Canadian Mineralogist, 19, 441–450.

Medenbach, O., Abraham, K., and Gebert, W. (1983) Molybdofornacit, ein neus Blei-Kupfer-Arsenat-Molybdat-Hydroxid von Tsumeb, Namibia. Neues Jahrbuch für Mineralogie, Monatshefte, 1983, 289–295.

Nespolo, M. and Ferraris, G. (2000) Twinning by syngonic and metric merohedry. Analysis, classification and effects on the diffraction pattern. Zeitschrift für Kristallographie, 215, 77–81.

Nickel, E.H. and Hitchen, G.J. (1994) The phosphate analog of molybdofornacite from Whim Creek, Western Australia. Mineralogical Record, 25, 203–204.

Orlandi, P., Pasero, M., and Bigi, S. (2010) Sardignaite, a new mineral, the second known bismuth molybdate: description and crystal structure. Mineralogy and Petrology, 100, 17–22.

Orlandi, P., Demartin, F., Pasero, M., Leverett, P. Williams, P.A., and Hibbs, D.E. (2011) Gelosaite, $BiMo^{6+}_{(2-5x)}Mo^{5+}_{6x}O_7(OH)\cdot H_2O$ ($0 \leq x \leq 0.4$), a new mineral from Su Senargiu (CA), Sardinia, Italy, and a second occurrence from Kingsgate, New England, Australia. American Mineralogist, 96, 268–273.

Orlandi, P., Gelosa, M., Bonacina, E., Caboni, F., Mamberti, M., Tanca, G.A., and Vinci, A. (2013) Sardignaite, gelosaite et tancaite-(Ce): trois nouveaux minéraux de Su Seinargiu, Sarroch, Sardaigne, Italie. Le Règne Minéral, 112, 39–52.

Patnaik, P. (2003) Handbook of Inorganic Chemicals, 931 p. McGraw-Hill, New York.

Plant, J.A., Simpson, P.R., Smith, B., and Windley, B.F. (1999) Uranium ore deposits – products of the radioactive Echo Bay U-Ni-Ag-Cu deposits, North West Territories, Canada. Economic Geology, 68, 635–656.

Pushcharovsky, D.Yu., Rastsvetaeva, R.K., and Sarp, H. (1998) Crystal structure of deloryite, $Cu_4(UO_2)[Mo_2O_8](OH)_6$. Journal of Alloys and Compounds, 239, 23–26.

Secco, L., Nestola, F., and Dal Negro, A. (2008) The wulfenite–stolzite series: centric or acentric structures? Mineralogical Magazine, 72, 987–990.

Shannon, R.D. (1976) Revised effective ionic radii and systematic studies of interatomic distances in halides and chalcogenides. Acta Crystallographica, A32, 751–767.

Sheldrick, G.M. (2008) A short history of SHELX. Acta Crystallographica, A64, 112–122.

Skvortsova, K.V. and Sidorenko, G.A. (1965) Sedovite, a new supergene mineral of uranium and molybdenum. Zapiski Vsesoyuznogo Mineralogicheskogo Obshchestva, 94, 548–554 (in Russian).

Strunz, H. and Nickel, E.H. (2001) Strunz Mineralogical Tables. 9th Edition, E. Schweizerbart Verlag, Stuttgart, 870 p.

Traverso, G.B. (1898) Sarrabus e i suoi minerali: note descrittive sui minerali del Sarrabus facienti parte della collezione di minerali italiani presso il Museo civico di Genova. Tipografia Sansoldi, Alba, Cuneo, 73 p.

Ünak, T. (2000) What is the potential use of thorium in the future energy production technology? Progress in Nuclear Energy, 37, 1–4.

Wilson, A.J.C. (1992) International Tables for X-ray Crystallography Volume C. Kluwer, Dordrecht.

Yang, H., Jenkins, R.A., Thompson, R.M., Downs, R.T., Evans, S.H., and Bloch, E.M. (2012) Markascherite, $Cu_3(MoO_4)(OH)_4$, a new mineral species polymorphic with szenicsite, from Copper Creek, Pinal County, Arizona, U.S.A. American Mineralogist, 97, 197–202.

Zelenski, M.E., Zubkova, N.V., Pekov, I.V., Polekhovsky, Y.S., and Pushcharovsky, D.Yu. (2012) Cupromolybdite, $Cu_3O(MoO_4)_2$, a new fumarolic mineral from the Tolbachik volcano, Kamchatka Peninsula, Russia. European Journal of Mineralogy, 24, 749–757.

Table captions

Table 1. Mineral species with Th as essential component. Chemical formulae after the IMA list (updated to October 2013).

Table 2. Microprobe analyses of ichnusaite (in wt%).

Table 3. X-ray powder diffraction data for ichnusaite.

Table 4. Crystal data and summary of parameters describing data collection and refinement for ichnusaite.

Table 5. Atomic positions and displacement parameters (in $Å^2$) for ichnusaite.

Table 6. Selected bond distances (in Å) for ichnusaite.

Table 7. O···O distances (in Å) and corresponding bond-valence values (in valence units, *v.u.*) calculated with parameters from Ferraris and Ivaldi (1988).

Table 8. Bond-valence values calculated with parameters from Brese & O'Keeffe (1991).

Table 9. Molybdate minerals containing the oxoanion $(MoO_4)^{2-}$.

Figure captions

Fig. 1. Ichnusaite, tabular crystals on {100}.

Fig. 2. Ichnusaite, crystal structure as seen down **c** (a) and **a** (b). Polyhedra: grey = Th-centered polyhedra; dark grey = Mo1 tetrahedra; white = Mo2 tetrahedra. Circles = interlayer H_2O groups. H_2O groups are not shown in (b).

Fig. 3. Hydrogen bond system in ichnusaite as seen down **c**. Polyhedra: grey = Th-centered polyhedra; dark grey = Mo1 tetrahedra; white = Mo2 tetrahedra. Circles: black = O2 site; dark grey = H_2O groups bonded to Th^{4+} cations (Ow6 and Ow10 sites); light grey = interlayer H_2O groups (Ow11 site).

Table 1. Mineral species with Th as essential component. Chemical formulae after the IMA list (updated to October 2013).

Mineral species	Chemical formula
Althupite	$AlTh(UO_2)_7(PO_4)_4(OH)_5 \cdot 15H_2O$
Aspedamite	$\square_{12}(Fe^{3+},Fe^{2+})_3Nb_4[Th(Nb,Fe^{3+})_{12}O_{42}](H_2O,OH)_{12}$
Cheralite	$CaTh(PO_4)_2$
Ciprianiite	$Ca_4(Th,REE)_2Al(B_4Si_4O_{22})(OH)_2$
Coutinhoite	$Th_xBa_{1-2x}(UO_2)_2Si_5O_{13} \cdot 3H_2O$
Ekanite	$Ca_2ThSi_8O_{20}$
Eylettersite	$Th_{0.75}Al_3(PO_4)_2(OH)_6$
Grayite	$(Th,Pb,Ca)PO_4 \cdot H_2O$
Huttonite	$ThSiO_4$
Ichnusaite	$Th(MoO_4)_2 \cdot 3H_2O$
Nuragheite	$Th(MoO_4)_2 \cdot H_2O$
Steacyite	$K_{0.3}(Na,Ca)_2ThSi_8O_{20}$
Thorbastnäsite	$ThCa(CO_3)_2F_2 \cdot 3H_2O$
Thorianite	ThO_2
Thorite	$ThSiO_4$
Thornasite	$Na_{12}Th_3(Si_8O_{19})_4 \cdot 18H_2O$
Thorogummite	$(Th,U^{6+})[(SiO_4), (OH)_4]$
Thorosteenstrupine	$(Ca,Th,Mn)_3Si_4O_{11}F \cdot 6H_2O$
Thorutite	$(Th,U,Ca)Ti_2(O,OH)_6$
Tuliokite	$Na_6BaTh(CO_3)_6 \cdot 6H_2O$
Turkestanite	$(K,\square)(Ca,Na)_2ThSi_8O_{20} \cdot nH_2O$
Umbozerite	$Na_3Sr_4ThSi_8(O,OH)_{24}$

Table 2. Microprobe analyses of ichnusaite (in wt%).

Oxide	1	2	3	4	average	e.s.d.	Ideal
MoO_3	49.85	47.17	46.54	47.87	47.86	1.43	47.51
ThO_2	42.28	43.42	43.89	44.01	43.40	0.79	43.57
Total	92.13	90.59	90.43	91.88	91.26	0.87	91.08

Table 3. Crystal data and summary of parameters describing data collection and refinement for ichnusaite.

Crystal data	
X-ray formula	$Th(MoO_4)_2 \cdot 3H_2O$
Crystal size (mm^3)	0.20 x 0.06 x 0.05
Cell setting, space group	Monoclinic, $P2_1/c$
a (Å)	9.6797(12)
b (Å)	10.3771(13)
c (Å)	9.3782(12)
β (°)	90.00(1)
V ($Å^3$)	942.0(2)
Z	4
Data collection and refinement	
Radiation, wavelength (Å)	Mo $K\alpha$, λ = 0.71073
Temperature (K)	293
$2\theta_{max}$	59.65
Measured reflections	4073
Unique reflections	2223
Reflections with $F_o > 4\sigma(F_o)$	2008
R_{int}	0.0279
$R\sigma$	0.0471
Range of h, k, l	$-10 \le h \le 13$, $-14 \le k \le 12$, $-12 \le l \le 5$
R [$F_o > 4\sigma(F_o)$]	0.0507
R (all data)	0.0603
wR (on F_o^2)	0.1461
Goof	1.128
Number of least-squares parameters	124
Maximum and minimum residual peak (e $Å^{-3}$)	6.91 (at 0.85 Å from Th) -3.17 (at 0.93 Å from Th)

Note: the weighting scheme is defined as $w = 1/[\sigma^2(F_o^2) + (aP)^2 + bP]$, with $P = [2F_c^2 + \text{Max}(F_o^2,0)]/3$. a and b values are 0.0699 and 53.6946.

Table 4. Atomic positions and displacement parameters (in Å^2) for ichnusaite.

Site	*x*	*y*	*z*	U_{eq}	U_{11}	U_{22}	U_{33}	U_{23}	U_{13}	U_{12}
Th	0.6781(1)	0.4625(1)	0.2364(1)	0.0127(2)	0.0251(3)	0.0035(2)	0.0095(3)	-0.0003(2)	-0.003(3)	-0.0002(2)
Mo1	0.5770(2)	0.7657(1)	-0.0092(2)	0.0142(3)	0.0278(8)	0.0034(7)	0.0112(7)	-0.0005(5)	0.0021(8)	-0.0010(6)
Mo2	0.7140(2)	0.4051(2)	-0.2074(2)	0.0155(4)	0.0282(9)	0.0057(6)	0.0125(8)	-0.0008(5)	0.0001(7)	-0.0008(6)
O1	0.546(1)	0.428(1)	-0.271(2)	0.021(3)	0.015(6)	0.016(6)	0.031(9)	-0.001(7)	0.004(7)	0.003(5)
O2	0.828(2)	0.519(1)	-0.282(2)	0.023(3)	0.031(8)	0.014(7)	0.025(8)	0.004(5)	-0.014(9)	0.002(6)
O3	0.699(2)	0.871(1)	-0.085(2)	0.019(3)	0.025(9)	0.019(7)	0.015(6)	0.008(5)	-0.002(7)	0.007(6)
O4	0.720(2)	0.420(1)	-0.020(2)	0.022(3)	0.041(10)	0.022(7)	0.005(6)	-0.002(5)	0.008(7)	-0.008(7)
O5	0.777(1)	0.250(1)	-0.264(2)	0.013(2)	0.011(5)	0.013(5)	0.017(6)	0.002(5)	0.011(6)	-0.002(5)
Ow6	0.863(2)	0.428(2)	0.430(2)	0.031(4)	0.055(13)	0.020(8)	0.019(8)	0.000(6)	-0.004(8)	0.008(8)
O7	0.442(2)	0.846(2)	0.076(2)	0.021(3)						
O8	0.510(2)	0.658(1)	-0.135(2)	0.021(3)	0.030(9)	0.017(7)	0.014(7)	-0.004(6)	-0.006(7)	0.002(7)
O9	0.668(2)	0.670(1)	0.111(2)	0.031(4)	0.065(13)	0.012(7)	0.015(7)	0.004(5)	0.006(9)	0.002(9)
Ow10	0.916(2)	0.539(2)	0.175(2)	0.033(4)	0.013(8)	0.049(12)	0.039(11)	0.016(8)	0.007(8)	0.000(8)
Ow11	0.030(2)	0.231(2)	0.536(2)	0.042(5)	0.048(12)	0.029(10)	0.049(13)	0.006(9)	-0.003(11)	-0.006(9)

Table 5. Selected bond distances (in Å) for ichnusaite.

Th	– O5	2.405(13)	Mo1	– O7	1.745(16)
	– O8	2.407(16)		– O9	1.746(18)
	– O3	2.412(14)		– O8	1.747(15)
	– O7	2.428(16)		– O3	1.765(16)
	– O9	2.450(15)			
	– O1	2.469(13)	Mo2	– O1	1.750(14)
	– O4	2.483(14)		– O4	1.760(14)
	– Ow10	2.505(17)		– O2	1.763(16)
	– Ow6	2.574(19)		– O5	1.800(13)

Table 6. X-ray powder diffraction data for ichnusaite.

I_{obs}	d_{obs} (Å)	I_{calc}	d_{calc} (Å)	*h k l*	I_{obs}	d_{obs} (Å)	I_{calc}	d_{calc} (Å)	*h k l*
mw	9.7*	100	9.68	1 0 0	vw	2.500*	1	2.500	0 4 1
w	7.03*	7	7.08	1 1 0	w	2.415*	2	2.413	-2 3 2
m	**5.66**	18	5.649	-1 1 1	mw	2.358	7	2.366	-3 2 2
		15	5.649	1 1 1			8	2.344	0 0 4
mw	5.19*	10	5.189	0 2 0	mw	2.284*	6	2.286	4 1 1
w	4.82*	12	4.840	2 0 0	mw	2.252*	5	2.255	1 3 3
mw	4.69*	16	4.689	0 0 2			1	2.221	-2 4 1
vw	4.12*	2	4.110	1 2 1	vw	2.212	1	2.210	-1 4 2
		15	3.973	2 1 1			1	2.194	-3 1 3
m	**3.930**	13	3.909	-1 1 2	vw	2.136	1	2.137	0 2 4
		11	3.909	1 1 2			1	2.136	4 2 1
s	**3.479***	45	3.479	0 2 2	w	2.097	2	2.092	-2 3 3
mw	3.365	12	3.367	-2 2 1			4	2.092	2 3 3
		14	3.367	2 2 1	w	2.055	3	2.060	3 2 3
		11	3.274	1 2 2			2	2.055	-2 4 2
s	**3.257**	23	3.257	1 3 0	w	2.024*	3	2.029	1 5 1
		10	3.203	-2 1 2	mw	1.980			
m	**3.074***	9	3.077	-1 3 1	w	1.937			
w	2.981*	4	2.993	0 1 3	mw	1.903			
w	2.866*	4	2.860	-1 1 3	m	1.861			
m	2.816*	13	2.814	2 3 0	w	1.813			
vw	2.741*	8	2.740	3 2 0	w	1.765			
mw	2.670*	4	2.675	-1 3 2	vw	1.733			
w	2.582*	1	2.581	1 2 3	w	1.700			
w	2.540*	6	2.546	2 1 3					

Notes: the d_{hkl} values were calculated on the basis of the unit cell refined by using single-crystal data. Intensities were calculated on the basis of the structural model using the software Powder Cell (Kraus and Nolze, 1996). Observed intensities were visually estimated. vs = very strong; s = strong; ms = medium-strong; m = medium; mw = medium-weak; w = weak; vw = very weak. Only reflections with I_{calc} > 5 are listed, if not observed.The strongest reflections are given in bold. Reflections used for the refinement of the unit-cell parameters are indicated by an asterisk.

Table 7. O···O distances (in Å) and corresponding bond-valence values (in valence units, *v.u.*) calculated with parameters from Ferraris and Ivaldi (1988).

O···O	*d* (Å)	vu
O2···Ow10	2.74(2)	0.21
Ow6···Ow11	2.79(3)	0.19
Ow10···Ow11	2.86(3)	0.16
O2···Ow6	2.88(2)	0.16

Table 8. Bond-valence values calculated with parameters from Brese & O'Keeffe (1991).

Site	O1	O2	O3	O4	O5	Ow6	O7	O8	O9	Ow10	Ow11	Σ (X – O)
Th	0.44		0.52	0.43	0.53	0.33	0.49	0.52	0.47	0.40		4.13
Mo1			1.47				1.55	1.54	1.55			6.11
Mo2	1.53	1.48		1.49	1.34							5.84
Σ (O – X)	1.97	1.48	1.99	1.92	1.87	0.33	2.04	2.06	2.02	0.40	0.00	
Σ (O – X)*	1.97	1.85	1.99	1.92	1.87	-0.02[1] 0.36[2]	2.04	2.06	2.02	0.35[1] 0.03[2]	0.03[1] -0.03[2]	
Species	O	O	O	O	O	H_2O	O	O	O	H_2O	H_2O	

*after correction for O···O hydrogen bonds. [1] Ow6 as donor and Ow10 as acceptor in the Ow6···Ow11···Ow10 hydrogen bond; [2] Ow6 as acceptor and Ow10 as donor in the Ow6···Ow11···Ow10 hydrogen bond.

Table 9. Molybdate minerals containing the oxoanion $(MoO_4)^{2-}$.

Mineral	Chemical formula	*a* (Å)	*b* (Å)	*c* (Å)	α (°)	β (°)	γ (°)	S.g.	Ref.
Cupromolybdite	$Cu_3O(MoO_4)_2$	7.664	6.867	14.555	90	90	90	*Pnma*	[1]
Ferrimolybdite	$Fe_2(MoO_4)_3{\cdot}nH_2O$	6.665	15.423	29.901	90	90	90	*Pmmn* *Pm*2$_1$*n*	[2]
Ichnusaite	$Th(MoO_4){\cdot}3H_2O$	9.680	10.377	9.378	90	90	90	*P*2$_1$/*c*	[3]
Lindgrenite	$Cu_3(MoO_4)_2(OH)_2$	5.61	14.03	5.40	90	98.4	90	*P*2$_1$/*n*	[4]
Markascherite	$Cu_3(MoO_4)(OH)_4$	9.990	5.993	5.526	90	97.4	90	*P*2$_1$/*m*	[5]
Molybdofornacite	$CuPb_2(MoO_4)(AsO_4)(OH)$	8.100	5.946	17.65	90	109.2	90	*P*2$_1$/*c*	[6]
Nuragheite	$Th(MoO_4){\cdot}H_2O$	7.358	10.544	9.489	90	91.9	90	*P*2$_1$/*c*	[7]
Powellite	$Ca(MoO_4)$	5.224	5.224	11.430	90	90	90	*I*4$_1$/*a*	[8]
Szenicsite	$Cu_3(MoO_4)(OH)_4$	8.520	12.545	6.079	90	90	90	*Pnnm*	[9]
Tancaite-(Ce)	$FeCe(MoO_4)_3{\cdot}3H_2O$	6.80	6.80	6.80	90	90	90	$Pm\bar{3}m$	[10]
Vergasovaite	$Cu_3(SO_4)(MoO_4,SO_4)O$	7.421	6.754	13.624	90	90	90	*Pnma*	[11]
Wulfenite	$Pb(MoO_4)$	5.433	5.433	12.098	90	90	90	*I*4$_1$/*a*	[12]

[1]Zelenski et al., 2012; [2] Horn et al., 1995; [3] this work; [4] Calvert and Barnes, 1957; [5] Yang et al., 2012; [6] Medenbach et al., 1983; [7] Orlandi et al., in preparation; [8] Aleksandrov et al., 1968; [9] Burns, 1998; [10] Bonaccorsi and Orlandi, 2010; [11] Berlepsch et al., 1999; [12] Secco et al. 2008.

533 **Fig. 1**. Ichnusaite, tabular crystals on {100}.

534
535

536 **Fig. 2**. Ichnusaite, crystal structure as seen down **c** (a) and **a** (b). Polyhedra: grey = Th-
537 centered polyhedra; dark grey = Mo1 tetrahedra; white = Mo2 tetrahedra. Circles = interlayer
538 H_2O groups. H_2O groups are not shown in (b).

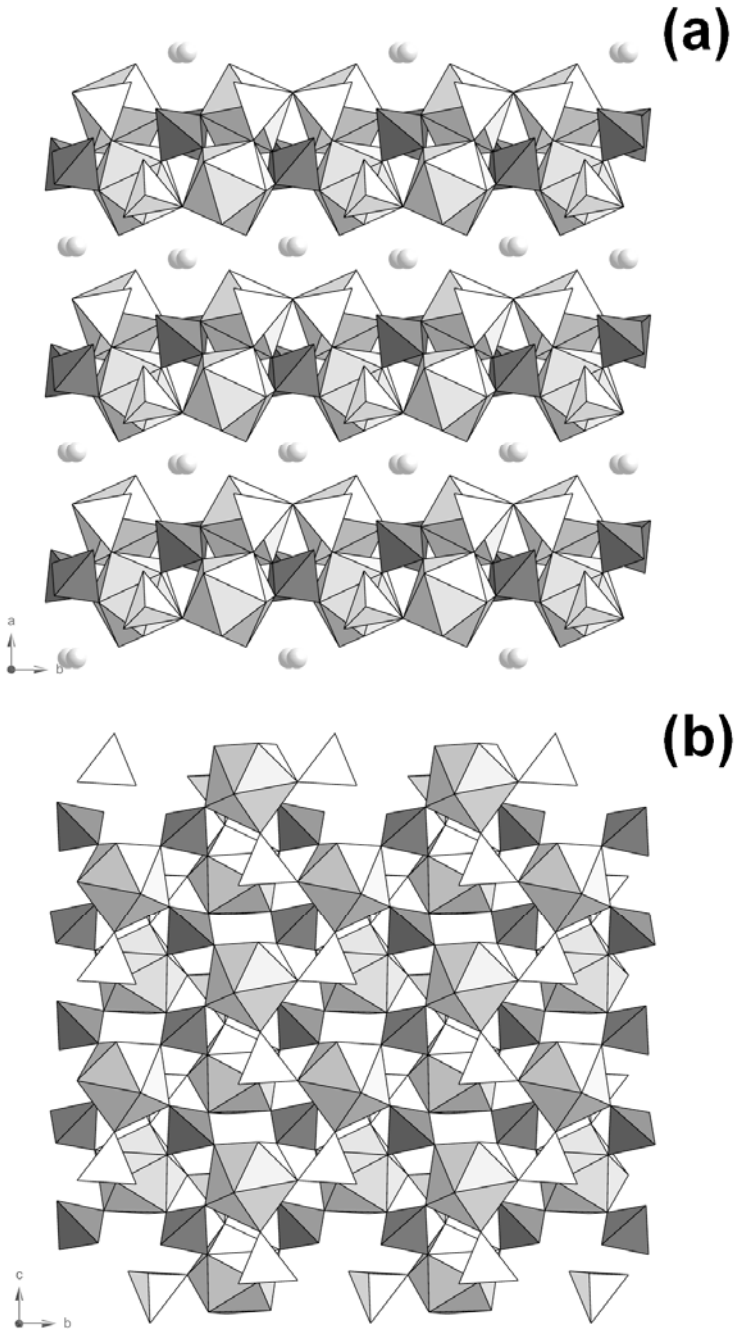

539
540
541

542 **Fig. 3**. Hydrogen bond system in ichnusaite as seen down **c**. Polyhedra: grey = Th-centered
543 polyhedra; dark grey = Mo1 tetrahedra; white = Mo2 tetrahedra. Circles: black = O2 site; dark
544 grey = H_2O groups bonded to Th^{4+} cations (Ow6 and Ow10 sites); light grey = interlayer
545 H_2O groups (Ow11 site).
546

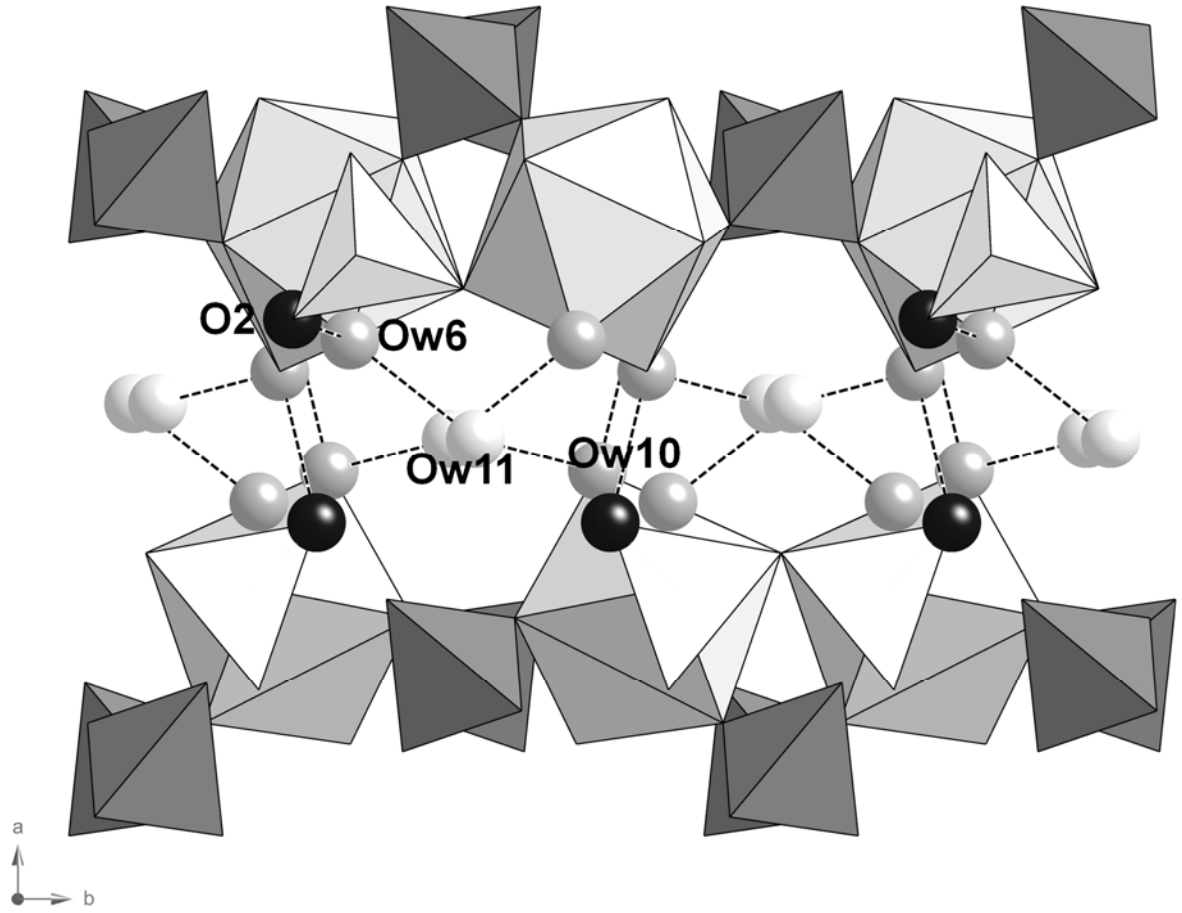

547


Sample 5334
BEI x100 WD28.96mm 10.00kV
200 µm

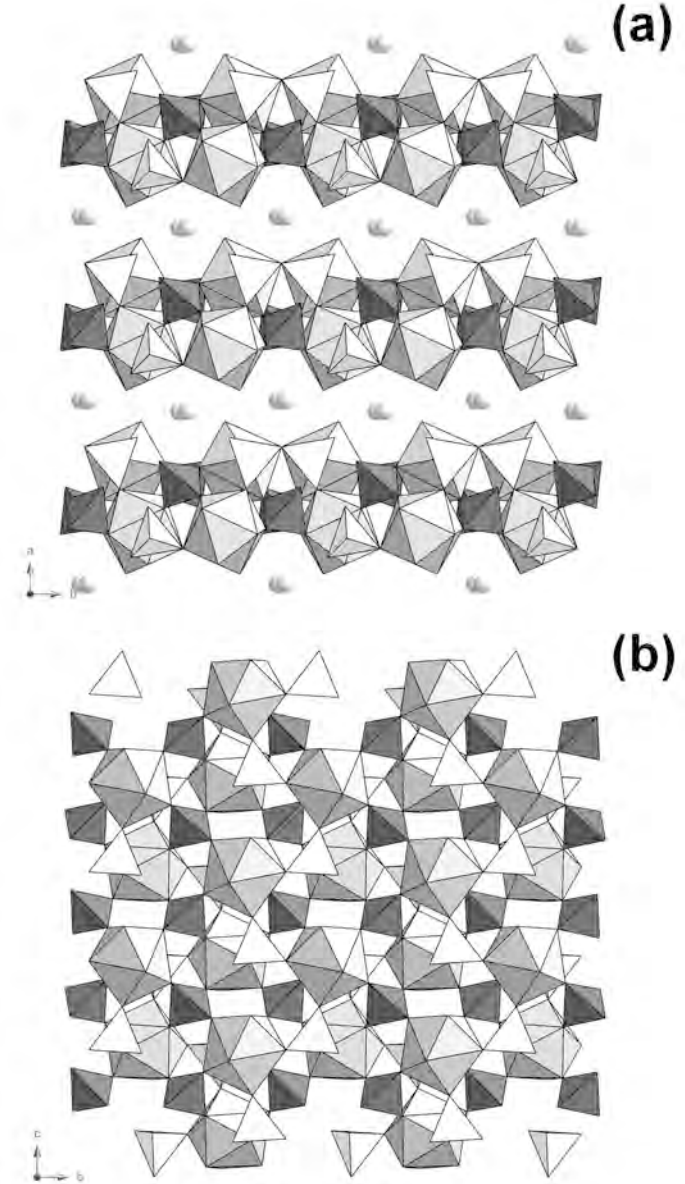
(a)
a
(b)
b

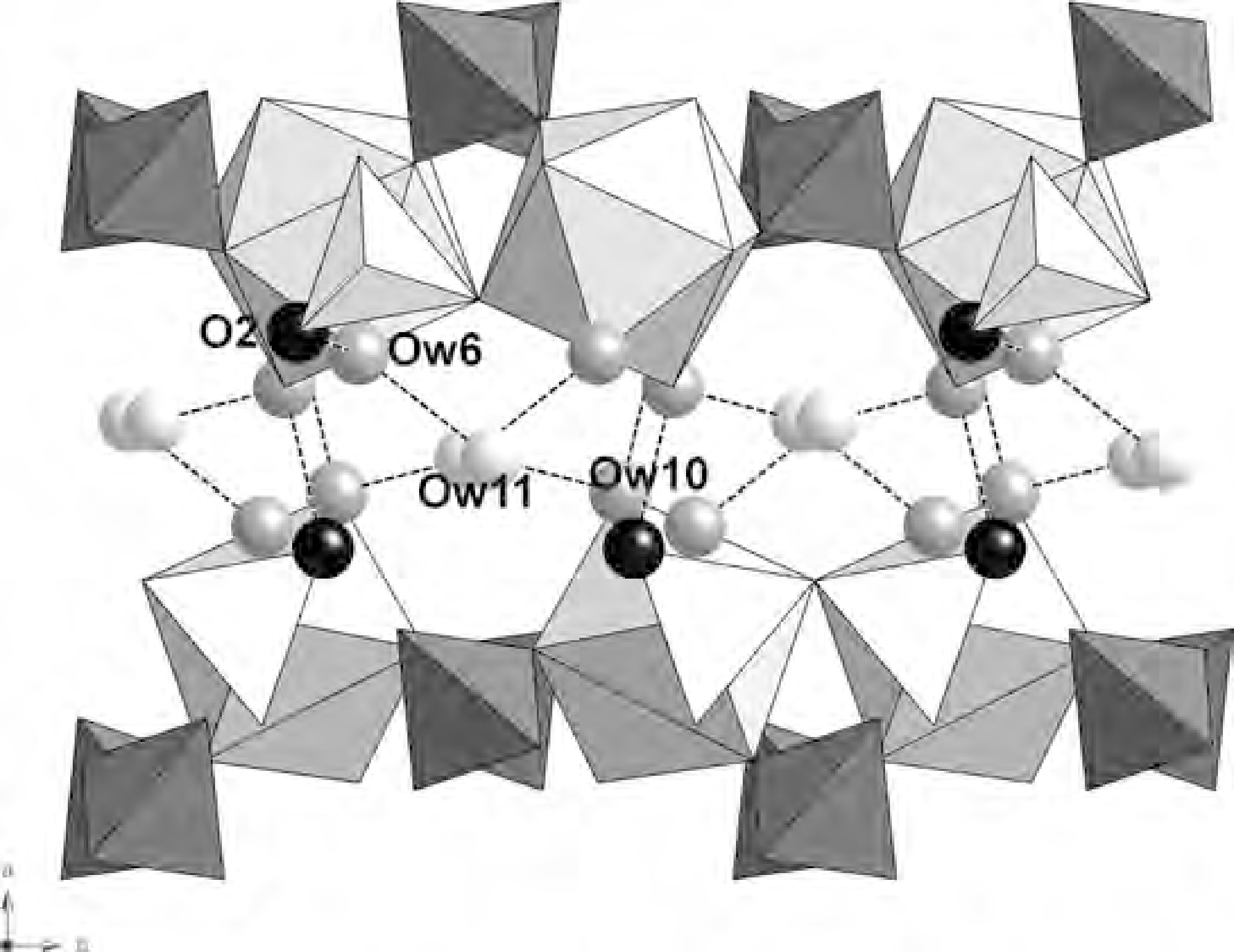
O2
Ow6
Ow11
Ow10